Indonesian Journal of Electrical Engineering and Informatics (IJEEI)
Vol. 13, No. 1, March 2025, pp. 57~68
ISSN: 2089-3272, DOI: 10.52549/ijeei.v13i1.6169

Improving Channel Gain of 6G Communications Systems Supported by Intelligent Reflective Surface

Abbas Thajeel Rhaif Alsahlanee[1], Jehan Kadhim Shareef Al-Safi [2]
[1] College of Education for Humanities, University of Thi-Qar, Nasiriyah, Thi-Qar, Iraq
[2] Department of Digital Media, Faculty of Media, University of Thi-Qar, Nasiriyah, Thi-Qar, Iraq

Article Info

Article history:

Received Dec 25, 2024
Revised Jan 28, 2025
Accepted Feb 16, 2025

Keyword:

Artificial intelligence
Energy efficiency
IRS
Metasurface
Reconfigurable intelligent surface
RIS
Transmission power

ABSTRACT

The 6G wireless communication networks may use intelligent reflecting surfaces (IRS). It can enhance energy efficiency (EE). The IRS can enhance wireless communication by selectively reflecting incident signals in favorable directions. A potential method to improve the efficacy of wireless channels is to use a software-controlled metasurface that reflects signals when the direct transmission line from the source to the destination is insufficient. The IRS may redesign the environment to facilitate radio signal transmission. The decrease in channel gain in 6G communications networks using multiple reflective elements of the IRS is one of the challenges. This study seeks to propose a solution to enhance the channel gain and performance of the IRS in 6G communication systems. The research aimed to improve channel gain in assisted-IRS 6G communication systems by artificial intelligence algorithm (DS-PSO: dynamic and static particle swarm optimization). This study's technique enhances the effectiveness of aided-IRS communication methods. The simulation results of the optimized IRS model proposed in this paper show a significant improvement in channel gain compared to the results of previous studies.

Corresponding Author:

Abbas Thajeel Rhaif Alsahlanee,
College of Education for Humanities,
University of Thi-Qar, Nasiriyah, Thi-Qar, Iraq.
Email: abbas.thajeell@gmail.com , abbas.thajeel@utq.edu.iq
ORCID Id: 0000-0003-1459-2214

1. INTRODUCTION

A new potential solution to the problems affecting 6G wireless communication networks is the intelligent reflecting surface (IRS), which may improve propagation conditions. Therefore, high route Line of Sight (LOS) effects are mitigated [1]. An intelligent radio environment has recently developed to meet the stringent criteria for communication and sensing imposed by future 6G systems [2]. In this approach, the digitally-controlled metasurface, also known as a reconfigurable intelligent surface (RIS) or IRS, wirelessly alters the propagation environment to enhance wireless communication and radar sensing [3], [4].

Metasurfaces are a novel type of functional materials containing artificially periodic or quasiperiodic structures on sub-wavelength length scales [5]–[7]. IRS metasurface unit cells have active elements that allow electrical adjustment of electromagnetic waves, making them programmable [6], [8]. Metasurfaces exhibit negative permittivity and permeability [6], [9]. Metasurfaces may change electromagnetic waves from microwave to visible light. The quality of wireless communications might change over time due to the unpredictable nature of radio propagation. During the propagation of electromagnetic waves, free-space route line-of-sights (LOSs), reflections, refractions, signal absorption, and diffractions induced by physical objects make wireless channels very dynamic [6], [10]. IRS's capacity to manipulate electromagnetic waves in real-time gives up endless possibilities to redirect the emphasis of wireless communications design from "adapting to wireless channels" to "modifying wireless channels." [10], [11]. In particular, IRS can achieve desirable functions by dynamically regulating phase shifts using

low-cost reflecting elements, including multi-antenna/MIMO (multiple-input multiple-output) channel rank improvement, environment obstacle avoidance, and reshaping channel realizations/distributions [12], [13].

Improved communication system performance is possible when transmit beamforming is used with an IRS that uses a phase-shift design [11], [14]. Another potential use of transmission beamforming technology is to generate several beams that may be directed toward nearby objects and people [11], [15].

To set up the IRS reflection pattern, or passive beamforming, for the sub-channels that connect the IRS to the wireless transceivers, channel state information (CSI) is required [8]. Unlike other wireless communication systems, the IRS has a more challenging estimating method since it is passive and cannot detect incident signals [6]. In contrast, by dynamically optimizing the phase, the IRS may strengthen the signal of the communications system [16].

On the other hand, the IRS may use Line of Sight (LOS) to link to the nearby target when trying to prevent the target from making a direct sensory link to the base station (BS). An extra line of sight (LOS) provided by the IRS shows the link between the base station (BS) and the target, allowing for object recognition from a different angle, which improves sensing effectiveness [13]. According to [17], a hybrid beam training and placement approach is used to assess the characteristics of the LOS paths for IRS-assisted mmWave communications. Thus, the IRS is well-positioned to establish LOS connections between the source and the destination. When there is an NLOS channel between the source and the destination, channel gain decreases. Certain circumstances call for an IRS to facilitate the transfer [18].

Multiple performance metrics, such as spectral efficiency (SE), transmit power, sum rate, throughput, security, and others, have been the focus of substantial research into the use of IRS in wireless communication [1], [19], [20]. In addition, the literature discussed the energy efficiency (EE) metric as a means of assessing the performance of IRS within wireless communication networks, as in [12], [20], [21].

Numerous prior studies have examined the channel gain of communication systems employing IRS [22]–[24]. Emil Björnson conducted a comparative analysis of the wireless channel's rate and energy efficiency for two different technologies: IRS and decode-and-forward (DF) relaying [18]. We have undertaken several recent studies employing artificial intelligence (AI) methodologies, including optimization algorithms, deep learning, and machine learning, to address complicated optimization challenges across diverse domains such as computer network and communication systems [25], the Internet of Things [26]–[28], recommender systems [29], [30], and design of prediction models [31]–[34].

This paper aims to enhance the channel gains of an IRS system for optimizing transmission performance in 6G communication systems. Optimization methods may be used to rearrange the IRS system, leading to enhanced performance of the newly generated models. The artificial intelligence algorithm (dynamic and static particle swarm optimization: DS-PSO) will be introduced to improve the efficacy of the standard IRS model. The efficacy of the IRS is contingent upon its channel gains between the source, the IRS, and the destination. The suggested optimization technique improves the channel gains of the source, standard IRS model, and destination. The improved channel gains dictate the efficacy of the optimized IRS model. The channel gains of an optimized IRS model are calculated using the equations specified in this suggested study.

The outline for the rest of this paper is as follows: The model of a system will be discussed in the next section. In Section 3, we will analyze the performance of the IRS model. In Section 4, we will explore the technical solution that was recommended for improving the model's performance. Section 5 will focus on the simulation results and numerical performance comparisons. In Section 6, conclusions will be given.

2. SYSTEM MODEL.

Here, we focus on one-to-one transmissions, where the source and destination each have a single antenna, where $h_{\mathrm{sd}} \in \mathbb{C}$ represents the deterministic flat-fading channel, while the destination receives the signal as in (1).

$$\mathrm{y} = h_{\mathrm{sd}}\sqrt{\mathrm{p}}\mathrm{s} + \mathrm{n} \tag{1}$$

where p represents the transmit power, s represents the unit-power information signal, and $\mathrm{n} \sim \mathcal{N}c(0, \sigma^2)$, represents the noise at the receiver. Antenna gains are included in the channels for convenience of notation. This single-input-single-output (SISO) channel has a capacity as in (2).

$$\mathrm{R}_{\mathrm{SISO}} = \log_2\left(1 + \frac{\mathrm{p}|h_{\mathrm{sd}}|^2}{\sigma^2}\right) \tag{2}$$

A higher transmission capacity during wireless communication can be achieved by using additional technologies. The IRS can be one of the technologies that enhance the data transmission capacity of wireless

communication systems. IRSs can outperform relays at processing deterministic flat-fading channels, channel estimation, and frequency-selective fading. In terms of performance, deterministic flat-fading channels achieve the best performance [18].

This paper examines the properties of the IRS. We enhance specific properties to achieve an optimized IRS model. Subsequently, we compare the standard and optimized IRS models to ascertain their strengths and weaknesses. To conduct this study, we created a comprehensive transmission diagram in the wireless communication system using either the standard IRS or the proposed optimized IRS, as shown in Figure 1.

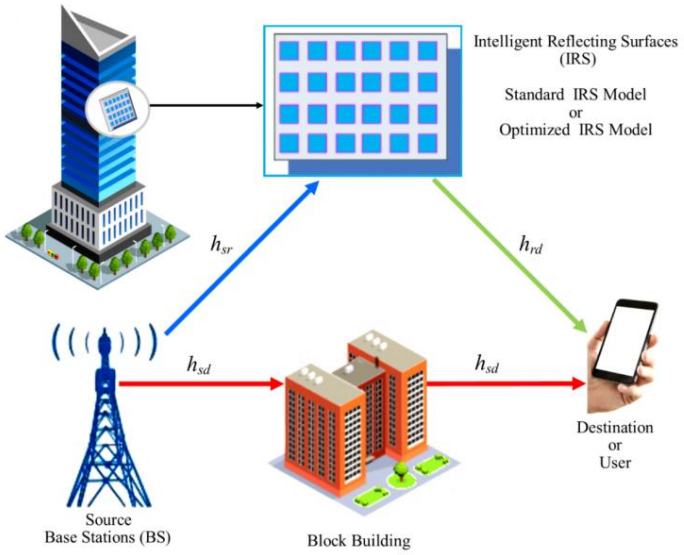

Figure 1. Standard IRS model/Optimized IRS model aided transmission.

2.1. The Transmission with The Support of The Standard IRS Model (IRS)

Discrete elements N exist in the standard IRS model (IRS), as shown in Fig. 1.; where $h_{\mathrm{sr}} \in \mathbb{C}^{\mathrm{N}}$ represents the source-to-IRS deterministic channel, and $[h_{\mathrm{sr}}]$n the nth element; $h_{\mathrm{rd}} \in \mathbb{C}^{\mathrm{N}}$, this specifies the channel that must be selected for the IRS to communicate with the destination. The diagonal matrix accurately represents the IRS's properties.

$$\Theta = \alpha \mathrm{diag}\left(e^{j\theta 1}, \ldots, e^{j\theta \mathrm{N}}\right) \tag{3}$$

where $\alpha \in [0,1]$ is the reflection coefficient at the fixed amplitude; $\theta_1, \ldots, \theta_{\mathrm{N}}$, these are the phase-shift parameters that may enhanced by IRS. The final destination's received signal within the IRS was calculated using the system model obtained in [35] (It was previously used in [18], [36], as in (4).

$$y_{\mathrm{IRS}} = (h_{\mathrm{sd}} + h_{\mathrm{sr}}^{\mathrm{T}} \Theta h_{\mathrm{rd}})\sqrt{\mathrm{ps}} + \mathrm{n} \tag{4}$$

using the same definitions for p, s, and n as used in the SISO case. With IRS-supported transmissions, channel estimation is non-trivial since the destination has perfect knowledge of the channels, and the phase-shift parameters can be enhanced. However, [37] describes some contemporary techniques. Specifically, the IRS-supported network has a channel capacity as in (5).

$$\mathrm{R}_{\mathrm{IRS}}(\mathrm{N}) = \max_{\theta_1,\ldots,\theta_{\mathrm{N}}} \log_2\left(1 + \frac{\mathrm{p}|h_{\mathrm{sd}} + h_{\mathrm{sr}}^{\mathrm{T}} \Theta \mathrm{h}_{\mathrm{rd}}|^2}{\sigma^2}\right) \tag{5}$$

$$= \log_2\left(1 + \frac{\mathrm{p}(|h_{\mathrm{sd}}| + \alpha \sum_{\mathrm{n}=1}^{\mathrm{N}} |[h_{\mathrm{sr}}]_{\mathrm{n}}[h_{\mathrm{rd}}]_{\mathrm{n}}|)^2}{\sigma^2}\right) \tag{6}$$

The rate expression in (5) will be obtained from the carrying capacity of a channel generating additive white Gaussian noise for any Θ. Take note that the essential factor is $h_{\mathrm{sr}}^{\mathrm{T}} \Theta h_{\mathrm{rd}} = \alpha \sum_{\mathrm{n}=1}^{\mathrm{N}} e^{j\theta \mathrm{n}} [h_{\mathrm{sr}}]_{\mathrm{n}} [h_{\mathrm{rd}}]_{\mathrm{n}}$. Following the same standard procedure as in [16] and [28], the maximum rate,

which represents the capacity, is achieved whenever the phase shifts are chosen as $\theta_n = \arg(h_{sd}) - \arg([h_{sr}]_n[h_{rd}]_n)$ to make each term in the sum have the same phase as h_{sd}.

2.2. The Transmission with The Support of The Optimized IRS Model (IRS^o).

In this paper, we present an improved version of the IRS model; it is the optimized IRS model (IRS^o) (shown in Fig. 1) utilizing one of the available optimization algorithms to surpass the performance and capabilities of the IRS.

The enhanced, as in the (7) diagonal matrix, shows the properties of the IRS^o, just like in the IRS, except for the value of N.

$$\Theta^o = \alpha \text{diag}\left(e^{j\theta_1}, \dots, e^{j\theta N^o}\right) \tag{7}$$

where the N^o is the N enhanced, phase-shifting variables that can be represented by $\theta_1, \dots, \theta_{N^o}$, these optimize through IRS^o. Furthermore, the final destination received the enhanced signal within the IRS^o will be as in (8).

$$y^o_{IRS} = (h_{sd} + h^T_{sr}\Theta^o h_{rd})\sqrt{p^o}s^o + n^o \tag{8}$$

where the p^o is the enhanced transmit power, the s^o is the unit-power information's enhanced signal, and the improved receiver noise will be represented by $n^o \sim \mathcal{N}c(0, \sigma^2)$. To analyze how the optimized model for the IRS affects the enhanced channel capacity in a network, we will use the expressions (9) and (10).

$$R^o_{IRS^o}(N^o) = \max_{\theta_1,\dots,\theta_{N^o}} \log_2\left(1 + \frac{p^o|h_{sd} + h^T_{sr}\Theta^o h_{rd}|^2}{\sigma^2}\right) \tag{9}$$

$$= \log_2\left(1 + \frac{p^o\left(|h_{sd}| + \alpha\sum_{n^o=1}^{N^o}|[h_{sr}]_{n^o}[h_{rd}]_{n^o}|\right)^2}{\sigma^2}\right) \tag{10}$$

Although the analysis in this paper simplifies by assuming deterministic channels, extending it to fading channels with complete channel information is straightforward. We need only consider predictions of the rate equations in (6) and (10). In light of this, all the conclusions also hold in this case.

Equations 7 to 10 are very similar to equations 3 to 6. Only the subscript "o" is added to $N, \Theta, p, s,$ and n. The difference between the equations is the addition of "o" to the symbols $N, \Theta, p, s,$ and n, which shows the effect of the optimization procedure on the standard versions. In this study, we will get results that are different from the results in the standard case.

3. PERFORMANCE OF ANALYTICS

Here, we analyze the three achievable rates discussed in the previous section. Uniquely, the phases of the channel elements ignore only the amplitudes used in the expressions. From now on, the notation $|h_{sd}| = \sqrt{\beta_{sd}}$, $|h_{sr}| = \sqrt{\beta_{sr}}$, $|h_{rd}| = \sqrt{\beta_{rd}}$, and $\frac{1}{N}\sum_{n=1}^{N}|[h_{sr}]_n[h_{rd}]_n| = \sqrt{\beta_{IRS}}$, will be introduced as a means of brevity within the IRS. However, the same notations will have different values with the IRS^o compared to the IRS, as follows $|h^o_{sd}| = \sqrt{\beta^o_{sd}}$, $|h^o_{sr}| = \sqrt{\beta^o_{sr}}$, $|h^o_{rd}| = \sqrt{\beta^o_{rd}}$, and $\frac{1}{N^o}\sum_{n^o=1}^{N^o}|[h^o_{sr}]_{n^o}[h^o_{rd}]_{n^o}| = \sqrt{\beta^o_{IRS^o}}$, where these notations are used to represent the IRS^o. The equations (2), (6), and (10) as follows must be reformulated for more compact forms.

$$R_{SISO} = \log_2\left(1 + \frac{p\beta_{sd}}{\sigma^2}\right) \tag{11}$$

$$R_{IRS}(N) = \log_2\left(1 + \frac{p\left(\sqrt{\beta_{sd}} + N\alpha\sqrt{\beta_{IRS}}\right)^2}{\sigma^2}\right) \tag{12}$$

$$R^o_{IRS^o}(N^o) = \log_2\left(1 + \frac{p^o\left(\sqrt{\beta^o_{sd}} + N^o\alpha\sqrt{\beta^o_{IRS}}\right)^2}{\sigma^2}\right) \tag{13}$$

Equality will be obtained for $N = 0$ with the IRS and for $N^o = 0$ with IRS^o, where $R_{IRS}(N)$ is an increasing function of N, while $R^o_{IRS^o}(N^o)$ is an increasing function of N^o; it is evident that $R^o_{IRS^o}(N^o) > R_{IRS}(N) \geq R_{SISO}$. As mentioned in [36] and elaborated on in [38] and [18], the rate increases as $\mathcal{O}(\log_2(N^2))$ when N becomes large. For this reason, for values of N, the exponential growth rate presented in this paper is $\mathcal{O}\left(\log_2\left(N^{o2}\right)\right)$. Consequently, it is not simple to evaluate the two cases of the IRS and the IRS^o.

The radio transmission will work enhanced within this paper's optimized IRS model compared to the IRS described in the previous literature. The transmission supported by the optimized IRS model has the highest rate for any $N > N^o \geq 1$ if $\beta_{sd} > \beta^o_{sd} > \beta^o_{sr}$; because the IRS-supported transmission provides the highest rate for $N \geq 1$ if $\beta_{sd} > \beta_{sr}$ compared to transmissions supported with any additional communications equipment [18], in which the optimized IRS model achieves the highest rate in the case of $\beta^o_{sd} \leq \beta^o_{sr} < \beta_{sd}$, while the IRS achieves the highest rate in the case of $\beta_{sd} \leq \beta_{sr}$.

As for the distinction between the transmission supported by the (IRS^o) and IRS; the IRS supports the case that $R_{IRS}(N) > R_{SISO}$ for $N \geq 1$ yield the highest rate if $R_{IRS}(N) > R_{ace}$; where any additional communications equipment will be represented by R_{ace}. Because the IRS supports multiple transmissions. $R_{SISO} > R_{ace}$ will cause this for $\beta_{sd} > \beta_{sr}$. As a consequence of this, the result will be $R_{IRS}(N) > R_{SISO} > R_{ace}$. But, this paper shows that ($R^o_{IRS^o}(N^o) > R_{SISO}$ for $N > N^o \geq 1$) in the case supported by the IRS^o, yields the highest rate if and only if $R^o_{IRS^o}(N^o) > R_{IRS}(N)$ achieves. Due to transmission supported by the IRS^o, $\beta_{sr} > \beta^o_{sd} > \beta^o_{sr}$ always occurs when $R_{SISO} < R_{IRS}(N)$. Therefore, the result will be $R^o_{IRS^o}(N^o) > R_{IRS}(N) > R_{SISO}$ in this case.

A LOS between the (IRS^o) and IRSs is required to interpret the resulting correctly IRS^o. Since any element in h_{sr} has the same magnitude as any element in h_{sr}, and h_{rd} has the same magnitude as any element in h_{rd}, it follows that the (IRS^o) elements all have the same magnitude as the essential IRS model elements. As a consequence of this, $\beta_{IRS} = \beta_{sr}\beta_{rd}$, and $\beta^o_{IRS} = \beta^o_{sr}\beta^o_{rd}$.

The higher rate of $\beta_{sd} > \beta_{sr}$ is provided by transmissions supported by the standard model of the IRS as in [18]. It is contrary to what is in this paper; the highest rate of $\beta_{sd} > \beta_{sr}$ is provided by transmissions supported by the optimized model of the IRS.

The difference between $R_{IRS}(N)$ and R_{SISO} is negligible for most actual values of N when the value is small for β_{rd} since $\sqrt{\beta_{sd}} \gg N\alpha\sqrt{\beta_{IRS}} = N\alpha\sqrt{\beta_{sr}\beta_{rd}}$. However, the difference in this paper is between $R_{IRS}(N)$, R_{SISO} and $R^o_{IRS^o}(N^o)$ is smallest since $\sqrt{\beta^o_{sd}} \gg N^o\alpha\sqrt{\beta^o_{IRS}} = N^o\alpha\sqrt{\beta^o_{sr}\beta^o_{rd}}$ for most practical values of N^o while β^o_{rd} is the smallest number for the most practical values of $\beta^o_{rd} < \beta_{rd}$. Note that a "large" channel gain in wireless communications is -50 dB. So, in case $\beta_{sd} \leq \beta_{sr}$, an IRS can give an appreciable performance gain, while in case $\beta^o_{sd} \leq \beta^o_{sr} < \beta_{sd}$, an (IRS^o) can provide an appreciable enhanced performance gain.

The numbers $p \to 0$ and $p^o \to 0$ have different values, given that $p \to 0$ achieved with $\beta_{sd} \leqslant \beta_{sr}$, while $p^o \to 0$ is achieved with $\beta^o_{sd} \leqslant \beta^o_{sr} < \beta_{sd}$, it can result in huge numbers. For example, (16) becomes $N > 963$ for $\alpha = 1, \beta_{sd} = -110$ dB, $\beta_{sr} = -80$ dB, and $\beta_{rd} = -60$ dB.

Suppose the destination demands a particular R_d. Then, suppose we use the formulas for the R_ds in (11), (12), and (13). Consequently, (13) is a non-convex optimization problem for the IRS. Since this optimization problem is non-convex, there is no conventional solution. Consequently, in this paper, we proposed a novel method based on the DS-PSO technique, which will be discussed in the next section.

4. THE PROPOSED TECHNICAL SOLUTION TO IMPROVE PERFORMANCE.

The IRS uses a method based on the DS-PSO technique to solve the non-convex optimization problem at (13). It is one of the hybrid PSO algorithms that use both dynamic and static particle swarm optimization (DS-PSO). The standard PSO algorithm uses a search space to initialize the particle swarm. The swarm subset, neighborhood, velocity, and random position are assigned per particle to keep track of the swarm's particles. Each particle in an algorithm performs a functional evaluation at its present position at every iteration. The current position becomes the particle's new personal best (Pos_{best}) if the current solution's fitness is better than the particle's current Pos_{best}. Equations (14) and (16) below update the particle's velocity and position. Since DS-PSO combines the topologies of dynamic and static versions for standard PSO, there is also a striking similarity between DS-PSO and PSO algorithms.

The primary distinction between the two algorithms is that DS-PSO assigns multiple topologies to each particle, one for dynamic and static neighborhoods. On the other hand, the additional dynamic designs intend to stimulate search space exploration rather than early convergence. A random topology is also generated during the algorithm implementation. On the other hand, the static topology preserves the standard PSO's exploitative properties that are absent in other dynamic PSO algorithms.

The neighborhood bests (N_{pbest}) of all the DS-PSO's topologies affect the particles, as swarm particles are updating their velocities (V) and positions (Pos) according to the equations (15) and (16).

$$\begin{aligned} Vel_{par}(i) = C_c[&Vel_{par}(i-1) + C_1R_1\left(Pos_{par}(i-1) - X_{par}(i-1)\right) \\ &+ C_2R_2\left(Nei_{parbest}(i-1) - X_{par}(i-1)\right) \end{aligned} \quad (14)$$

$$\begin{aligned} V_{par}(i) = C_c[&V_{par}(i-1) + C_1R_1\left(Pos_{par}(i-1) - X_{par}(i-1)\right) \\ &+ C_2R_2\left(D_{parbest}(i-1) - X_{par}(i-1)\right) \\ &+ C_3R_3\left(S_{parbest}(i-1) - X_{par}(i-1)\right)] \end{aligned} \quad (15)$$

$$X_{par}(i) = X_{par}(i-1) + V_{par}(i) \quad (16)$$

The above equations $V_{par}(i)$ represent the velocity, and The particle's (par) position at the current iteration i is denoted by $X_{par}(i)$. The particle, personal, dynamic, and static enhanced solutions identified up to this point in iteration i are denoted by $Pos_{par}(i)$, $D_{parbest}(i)$ and $S_{parbest}(i)$.

The constriction coefficient, commonly set to around 0.7298438 to avoid exploding velocities, is denoted by C_c. In eq. (14), C_1 and C_2 represent acceleration coefficients that increase particle attraction to Pos_{par} and $N_{parbest}$, respectively. Standard PSO has acceleration coefficients. C_1 and C_2 of 2.05 per one and a total acceleration coefficient of 4.1. Additionally, C_1, C_2 and C_3 represent acceleration coefficients used in eq. (15) to increase particle attraction to $Pos_{par}(i)$, $D_{parbest}(i)$ and $S_{parbest}(i)$, respectively. Each particle will draw to the optimum static, dynamic, and personal performance. Therefore, the DS-PSO algorithm finds three acceleration coefficients rather than the standard PSO algorithm's two acceleration coefficients. These coefficients of acceleration are C_1, C_2, and C_3; also, set to 4.1/3, so that per coefficient 1.366666667.

To encourage exploration, per of the velocity equation position elements is multiplied with the vector of R_1, R_2, and R_3 randomly generated values, which are in the range [0,1]. Each element of V_{par} must be kept within a $[V_{min}; V_{max}]$, range to keep particles contained within the search space, where $[V_{min}; V_{max}]$ is the search space's minimum and maximum values. Instead of being impacted by one neighborhood's best $N_{parbest}$, the particle is prejudiced for $D_{parbest}$ and $S_{parbest}$. Therefore, this will be the best solution with particles' dynamic and static topologies [39]–[44].

The pseudocode flow of the sequence of operations of the DS-PSO algorithm is shown in [39], [40], [44].

Table 1. The main parameters used in the DS-PSO algorithm.

Parameter	Value
Iteration (i)	1000
Particles (par)	10
coefficients of acceleration ($C_1 = C_2 = C_3$)	4.1/3
The minimum probability of restructuring neighborhoods	0.1
The maximum probability of restructuring neighborhoods	0.2
Intervals for the probability of restructuring neighborhoods	0.5
Intertie coefficient (spaced frequency points)	1
The search space's minimum values (V_{min})	1
The search space's maximum values (V_{max})	70

5. SIMULATION RESULTS AND NUMERICAL PERFORMANCE COMPARISON.

This section assesses the appropriateness of approximate outcomes by ascertaining the channel gains, which determine the selection between a standard IRS model and an optimized IRS model. It determines whether the experimental setups employed in Section 3 function in the high or low SNR regime. A numerical analysis of the systems will be conducted. Subsequently, the EE of the transmission aided by the optimized IRS model is computed using the mathematical equations mentioned in Section 3 of this article. A comparative analysis is then conducted using the findings of previous research studies.

The 3GPP Urban Micro (UMi) model, as described in reference [48], is employed with the carrier frequency set at 3 GHz to depict the channel gains accurately. The line-of-sight (LOS) and non-line-of-sight (NLOS) versions of UMi, specified in the distance≥ 10 m, are used. Let us say that the antenna gains for the

transmitter and receiver, measured in dBi, are G_t and G_r, respectively. It is possible to use UMi at both LOS and NLOS distances.

Channel gain values for the UMi (LOS, NLOS) versions are calculated using (17) with the given values for G_t and G_r, and d. Then, optimization is conducted on the channel gain values utilizing the UMi versions LOS to attain the enhanced channel gain. The paper's proposed optimization algorithm enhances the channel gain values with the UMi-LOS version. The simulation obtained new channel gain values, or optimized UMi-LOS, achieved through optimization. The channel gain value in the optimized UMi-LOS version can be calculated using (18).

$$\beta(d)[\mathrm{dB}] = G_t + G_r + \begin{cases} -37.5 - 22\log_{10}\left(\frac{d}{1\ \mathrm{m}}\right) & \text{if LOS} \\ -35.1 - 36.7\log_{10}\left(\frac{d}{1\ \mathrm{m}}\right) & \text{if NLOS} \end{cases} \quad (17)$$

$$\beta^{o}(d)[\mathrm{dB}] = \mathrm{Optimized}\ [G_t + G_r + \{-37.-22\log_{10}\left(\frac{d}{1\ \mathrm{m}}\right)\}] \quad \text{if Optimized LOS} \quad (18)$$

Our hypothesis posits that the deterministic model assumes uniform antenna gains of 5 dBi for both the transmitter and receiver ($G_t = G_r$) within a distance of 100 meters while disregarding shadow fading.

Simulation is conducted to evaluate the channel gain β according to the UMi versions (UMi-LOS, UMi-NLOS, and LOS with the optimization algorithm proposed in this paper (Optimized UMi-LOS)), as depicted in Fig. 2 and 3. The simulation requires identical parameters for all three versions. Figures 2 and 3 illustrate the relationship between channel gain values (-110 dBi to -40 dBi) and distances (10 to 100 meters) for different UMi versions (UMi-LOS, UMi-NLOS, and Optimized UMi-LOS).

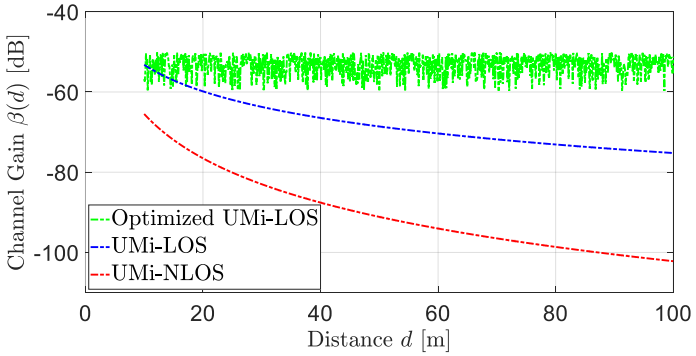

Figure 2. Gains of a typical channel as a distance function.

Figure 2 highlights the channel gain magnitude for nominal values ranging from -110 dBi to -50 dBi. The mean values range from -110 dBi to -50 dBi, depending on the UMi versions, which include LOS, NLOS, and optimized LOS. The channel gains show distance-dependent variability in three different ranges: (-60 dBi to -50 dBi) with optimized UMi-LOS, (-80 dBi to -50 dBi) with UMi-LOS, and (-110 dBi to -50 dBi) with UMi-NLOS. Since the channel gain values change depending on the UMi version and the distance, Figure 3 illustrates Figure 2.

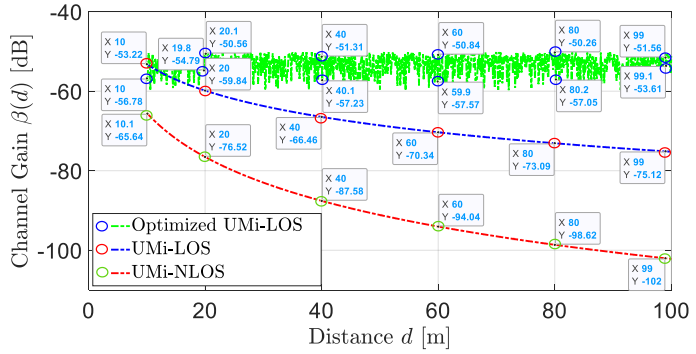

Figure 3. Illustration of gains of a typical channel as a distance function.

Figure 3 provides a more detailed representation of the simulation of channel gain in comparison to the distance function. We collected ten samples of channel gain values for the UMi-Optimized Line-of-Sight (LOS) version based on varying distances. The samples were divided into two categories, each containing five samples. We collected five samples from the first category and five samples from the second category of the UMi-Optimized LOS version within the same range; this was done to determine the channel gain values at specific distances. The distance between the first and one of the second five samples is between 0.1 and 0.3 meters. Table 1 was created to compare the channel gain values within the UMi-Optimized LOS issuance range using the sample values shown in Figure 3.

Table 2. The channel gain values based on the distance for the UMi-Optimized (LOS) version.

Sample No.	Category No.	Distance (d)	Channel gain
Sample 1	First	19.8	-54.79
	Second	20.1	-50.56
Sample 2	First	40	-51.31
	Second	40.1	-57.23
Sample 3	First	59.9	-57.57
	Second	60	-50.84
Sample 4	First	80	-50.26
	Second	80.2	-57.05
Sample 5	First	99	-51.56
	Second	99.1	-53.61

Table 1 shows that the ten samples collected for the initial version (UMi-Optimized LOS) ranged from 19.8 to 99.1 meters in distance; every pair of samples among the exhibited proximity. Table 1 reveals that adjacent samples are within a distance of less than 0.3 meters. However, the channel gain values vary between each sample. The channel gain reached its maximum value of -50.26 at a distance of 80 meters. The channel gain was -57.05 at a distance of 0.2 meters, relative to the highest channel gain value observed at a distance of 80.2 meters. However, the channel gain reached its minimum value of -57.57, observed at 59.9 meters. In comparison, the channel gain was -50.84 at a distance of 0.1 meters, relative to the lowest channel gain value at a distance of 60 meters.

As a result, the channel gain values for the UMi-Optimized LOS version ranged from -50.26 to -57.57; this suggests that short distances, rather than long ones, affect the channel gain values. Thus, the channel gain values remain within the range regardless of the increase in distance.

Six samples were collected for each of the three variations of UMi (UMi-Optimized LOS, UMi-LOS, UMi-NLOS) at distances of 10 m, 20 m, 30 m, 40 m, 60 m, 80 m, and 99 m, as shown in Figure 3. Table 2 presents the channel gain values for the three UMi versions, facilitating a comparative analysis.

Table 3. The channel gain values for different versions of UMi based on distance.

Sample No. of Distance (d)	Sample 1	Sample 2	Sample 3	Sample 4	Sample 5	Sample 6
Distance (d)	10	20.1	40	60	80	99
Channel gains with UMi-NLOS	-65.64	-76.52	-87.58	-94.04	-98.62	-102
Channel gains with UMi-LOS	-56.78	-59.84	-66.46	-70.34	-73.09	-75.12
Channel gains with Optimized UMi-LOS	-53.22	-54.79	-51.31	-57.57	-50.26	-51.56

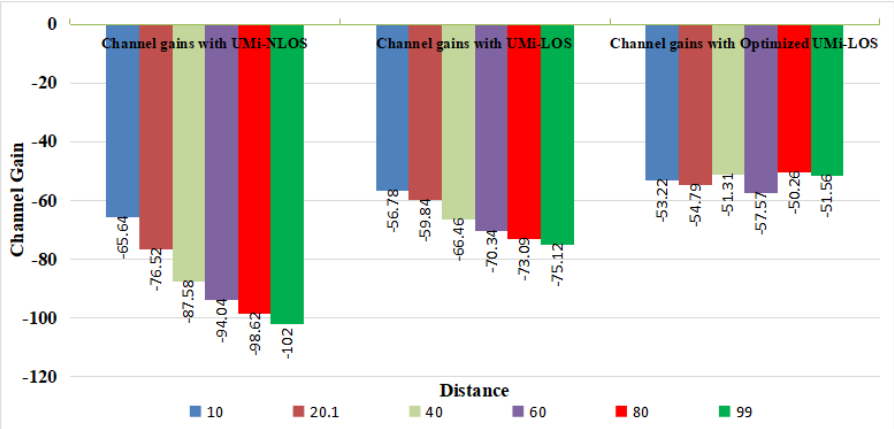

Figure 4. The channel gain values for different versions of UMi based on distance.

Table 2 and Figure 4 display the channel gain and distance measurements obtained from the samples extracted from Figure 3. The samples demonstrated variations in channel gain values based on the MUi

version and distance. The channel gain values in the UMi-NLOS version decreased as the distance increased, as indicated by Figure 3 and Table 2. The channel gain values initially measured -65.64 at a distance of 10 meters and subsequently exhibited a gradual decrease. The distance between the transmitter and receiver gradually increased until reaching a value of -102 for the channel gain at 99 meters. Based on this observation, it can be concluded that the channel gain values within the UMi-NLOS version band are influenced by increasing the distance .

Furthermore, it is observed that the channel gain values in Figure 3 and Table 2 for the UMi-LOS version are variable. The channel gain values of these samples exhibit a negative correlation with distance. In the UMi-LOS version, the channel gain values were -56.78 dB at a distance of 10 meters. The channel gain values gradually decreased with increasing distance, reaching a final value of -75.12 at 99 meters. Based on this observation, it can be concluded that the channel gain values within the UMi-LOS version range are influenced by increasing the distance.

The channel gain values in the UMi-NLOS version were lower than those in the UMi-LOS version, which can be attributed to the distance. The channel gain values of the UMi-LOS version are superior to those of the UMi-NLOS version.

This paper's proposed version (UMi-Optimized LOS) had channel gain values ranging from -50.26 to -57.57. The channel gain values for the UMi-Optimized LOS version within the distance range of 10 to 99 meters are depicted in Figure 3 and Table 2. The channel gain values in the UMi-Optimized LOS version exhibited instability, unlike the UMi-LOS and UMi-NLOS versions. The channel gain values in the UMi-Optimized LOS version do not exhibit a decrease with increasing distance. However, they vary across different samples, with some showing a decrease and others showing an increase.

The channel gain values for the UMi-Optimized LOS version were -53.22 dB at a distance of 10 meters, -54.79 dB at a distance of 20 meters, -51.31 dB at a distance of 40 meters, and -57.57 dB at a distance of 60 meters. Subsequently, the values increased to -50.26 and -51.56 at distances of 80 and 99 meters, respectively .

Based on our analysis, it can be concluded that the channel gain values remain unaffected within the specified range of the version (UMi-Optimized LOS) when the distance is increased. The channel gain values in the UMi-Optimized LOS version exhibit a continuous decrease and rise pattern within a specific range of values (-57.57 to -50.26). This pattern remains consistent regardless of the distance within this range.

The channel gain values in the UMi-Optimized LOS version were higher than those in the UMi-LOS and UMi-NLOS versions despite the distance impacting the channel gain values. The channel gain values of the UMi-Optimized LOS version are superior to those of the UMi-LOS and UMi-NLOS versions.

The highest channel gain values for the three versions of UMi (UMi-Optimized LOS, UMi-LOS, UMi-NLOS) within the distance range of 10 to 100 meters in this study are -50.26. The version proposed in this paper, UMi-Optimized LOS, has the highest channel gain value. The channel gain value for the UMi-Optimized LOS version is superior to that for the UMi-LOS and UMi-NLOS versions, which were -56.78 and -65.64, respectively, at their highest point .

Similarly, the proposed version (UMi-Optimized LOS) has a minimum channel gain value of -57.57. The channel gain of UMi-Optimized LOS is superior to that of UMi-LOS and UMi-NLOS versions, with values of -75.12 and -102, respectively, at the lowest level .Therefore, the UMi-Optimized LOS version described in this study outperforms the UMi-LOS and UMi-NLOS versions in terms of the maximum and minimum channel gain values, respectively.

Hence, we recommend applying the proposed method in this study to enhance transmission performance in 6G networks with the aid of programmed IRS.

Comparing the proposed optimized IRS model in this paper with competing models from previous studies regarding channel gains indicates that the optimized IRS model outperforms the competing models.

Table 4. Comparison of Channel Gain Values Across UMi Versions and Previous Studies.

Parameter	**UMi-NLOS**	**UMi-LOS**	**Previous Study 1** [22]	**Previous Study 2** [22]	**Previous Study 3** [23]	**Previous Study 4** [24]	**Optimized UMi-LOS (Proposed)**
Channel Gain Range (dB)	-102 to -65.64	-75.12 to -56.78	-160 to -60.6	-160 to -63.6	-90 to -72.6	-60 to -0.1	-57.57 to -50.26
Distance Range (m)	10 to 99	10 to 99	0 to 25.4	0 to 11.4	1 to 3	0.01 to 0.1	10 to 99
Max Channel Gain (dB)	-65.64	-56.78	-60.6	-63.6	-72.6	-0.1	-50.26
Min Channel Gain (dB)	-102	-75.12	-160	-160	-90	-60	-57.57
Trend with Distance	Decreases	Decreases	Decreases	Decreases	Decreases	Decreases	Fluctuates within a range
Performance	Lowest	Moderate	Moderate	Moderate	Moderate	Moderate	Highest

The channel gains for the three Urban Microcell (UMi) model versions are compared in Table 2. This study includes UMi-NLOS, UMi-LOS, and the optimized version of UMi-LOS. It also compares the results of the present study with those of three previous studies that were published in 2024 and 2025 ([22]–[24]). In terms of channel gain, the study shows the advantages of the optimized version of UMi-LOS.

The range of Channel Gain:

UMi-NLOS: Channel gain values for UMi-NLOS range from -102 dB to -65.64 dB, indicating significant signal attenuation due to reflections and obstacles in a non-line-of-sight setting. Previous studies ([22]–[24]), which similarly acknowledge significant attenuation in NOLS settings, correspond with this range.

The UMi-LOS variation exhibits a limited range of -75.12 dB to -56.78 dB, signifying enhanced signal transmission in the absence of obstructions; this aligns with prior research indicating that channel gain is often superior under LOS conditions compared to NLOS conditions. As shown by prior research, the UMi-LOS variations achieve channel gain values ranging from -160 dB to -0.1 dB.

UMi-LOS with Enhancements: The recommended UMi-LOS version yields optimal results with channel gain levels ranging from -57.57 dB to -50.26 dB. The LOS version's optimization technique, which enhances signal strength and reduces attenuation, accounts for this rise. The optimized version surpasses both UMi-LOS and UMi-NLOS, in addition to exceeding the results of prior studies.

Distance Dependency: A negative connection between channel gain and distance is evident in both UMi-NLOS and UMi-LOS circumstances. The inverse-square law of signal propagation states that channel gain decreases with increasing distance. This trend has also been observed in previous studies ([22]–[24]). **Optimized UMi-LOS**: Unlike the other versions, the Optimized UMi-LOS does not show a consistent decrease in channel gain with increasing distance. Instead, the channel gain fluctuates within a narrow range (-57.57 dB to -50.26 dB), indicating that the optimization algorithm mitigates the impact of distance on signal attenuation; this is a significant improvement over the traditional UMi-LOS and UMi-NLOS versions, as well as UMi-LOS, in the results reported in previous studies.

Maximum and Minimum Channel Gain: The maximum channel gain for the Optimized UMi-LOS (-50.26 dB) is significantly higher than that of UMi-LOS (-56.78 dB) and UMi-NLOS (-65.64 dB). It also surpasses the maximum channel gains reported in previous studies ([22]: -60.6 dB and -63.6 dB, [23]: -72.6 dB, [24]: -0.1 dB). Similarly, the minimum channel gain for the Optimized UMi-LOS (-57.57 dB) is higher than that of UMi-LOS (-75.12 dB) and UMi-NLOS (-102 dB), as well as the minimum values from previous studies ([22]: -160 dB, [23]: -90 dB, [24]: -60 dB); this demonstrates the robustness of the proposed optimization algorithm in maintaining higher channel gains across varying distances.

Performance Comparison: The improved UMi-LOS version consistently surpasses the results of prior studies, as well as UMi-LOS and UMi-NLOS; this improves transmission performance in 6G networks by achieving enhanced channel augmentation while reducing distance dependence. The UMi-LOS works better than the new version if it has a higher channel gain than the UMi-NLOS. Distance-related attenuation still limits non-line-of-sight conditions despite being consistent with studies that demonstrate the superiority of LOS conditions. The study confirms the poor UMi-NLOS version, as also observed in previous studies, due to the influence of distance and limited channel gains.

Implications for 6G Networks: Using the improved UMi-LOS proposed in this paper helps to improve the performance of next-generation networks in an unprecedented way, even when these networks are combined with surfaces. The distance dependence will be reduced while ensuring high channel gain, thus improving network coverage, data rate, and reliability. The inadequacy of the standard UMi-LOS and UMi-NLOS has been proven in this study due to the weak influence of the surrounding environment and distance. The improved version proposed in this paper has greatly helped to solve these problems, so it can be considered the best model for 6G communication systems.

Based on the study's results, the proposed UMi-LOS in this paper is different from previous versions and helps revolutionize channel modeling for next-generation networks even when combined with IRS. Comparing it with recent references ([22]–[24]) from 2024 and 2025 provides a reliable basis for comparison, demonstrating the compatibility of this study with new research trends.

6. CONCLUSION

This paper presents two IRS models: the standard model and an improved version utilizing an intelligent optimization technique. This study proves that optimization approaches improve the IRS's performance by successfully implementing the proposed optimization technique. Therefore, we designed an improved version of the optimized IRS form. Subsequently, a comparison was conducted between the standard IRS model and the optimized IRS model, showing that the latter shows superior channel gains. This paper's proposed optimized IRS model consists of reflective elements that transmit power from the source to the destination through two channels. Each reflecting element has a channel gain from the source to the

optimized IRS and another from the optimized IRS to the user or destination. The IRS requires several reflective elements to address the problem of minimal channel gain. Optimizing channel gain reduces the number of reflective elements, a strength in the optimized IRS design. This study compares the optimized IRS model proposed in this paper with the IRS and RIS models previously suggested in other studies, considering that IRS is referred to as RIS in some previous studies. Compared to previous studies, the optimized IRS model described in this study enhances channel gains.

REFERENCES

[1] K. Aswini and M. Surendar, "Performance analyses of intelligent reflecting surface aided downlink multi-user rate-splitting multiple access system for 6G applications," *Comput. Networks*, vol. 242, p. 110271, 2024.

[2] D. Sarkar, V. Pal, S. S. Yadav, and S. K. Patra, "IRS-aided NOMA-based communication architecture for 6G wireless networks: An enhanced error-control and reliable data transmission," *Phys. Commun.*, vol. 65, p. 102394, 2024.

[3] J. Wang *et al.*, "Reconfigurable intelligent surface: Power consumption modeling and practical measurement validation," *IEEE Trans. Commun.*, 2024.

[4] X. Wang, L. Feng, F. Zhou, and W. Li, "Coverage and reliability analysis of multi-IRS-aided distributed space–time block coding in MISO wireless communication systems," *Phys. Commun.*, vol. 63, p. 102311, 2024.

[5] S. Sharma, A. K. Mishra, M. H. Kumar, K. Deka, and V. Bhatia, "IRS-Enhanced Cooperative NOMA: A Contemporary Review," *IEEE Access*, 2024.

[6] W. Wang and W. Zhang, "Intelligent reflecting surface configurations for smart radio using deep reinforcement learning," *IEEE J. Sel. Areas Commun.*, vol. 40, no. 8, pp. 2335–2346, 2022.

[7] T. J. Cui, M. Q. Qi, X. Wan, J. Zhao, and Q. Cheng, "Coding metamaterials, digital metamaterials and programmable metamaterials," *Light Sci. Appl.*, vol. 3, no. 10, pp. e218–e218, 2014.

[8] C. N. Efrem and I. Krikidis, "Robust IRS-Element Activation for Energy Efficiency Optimization in IRS-Assisted Communication Systems With Imperfect CSI," *IEEE Trans. Wirel. Commun.*, 2024.

[9] X. Shao, C. You, and R. Zhang, "Intelligent reflecting surface aided wireless sensing: Applications and design issues," *IEEE Wirel. Commun.*, 2024.

[10] C. N. Efrem and I. Krikidis, "Robust IRS-Element Activation for Energy Efficiency Optimization in IRS-Assisted Communication Systems With Imperfect CSI," *IEEE Trans. Wirel. Commun.*, vol. PP, no. May, p. 1, 2024.

[11] X. Liu, H. Zhang, K. Long, M. Zhou, Y. Li, and H. V. Poor, "Proximal policy optimization-based transmit beamforming and phase-shift design in an IRS-aided ISAC system for the THz band," *IEEE J. Sel. Areas Commun.*, vol. 40, no. 7, pp. 2056–2069, 2022.

[12] H. Liu, N. Qi, K. Wang, T. A. Tsiftsis, W. Wang, and Y. Liu, "Network deployment with energy efficiency optimization in IRS-assisted cell-free MIMO system," *Phys. Commun.*, vol. 63, p. 102287, 2024.

[13] X. Shao, C. You, W. Ma, X. Chen, and R. Zhang, "Target sensing with intelligent reflecting surface: Architecture and performance," *IEEE J. Sel. Areas Commun.*, vol. 40, no. 7, pp. 2070–2084, 2022.

[14] G. R. Mati and S. Das, "Orthonormal pilot-based channel estimation with low complexity phase shift optimization and coverage enhancement for IRS-assisted B5G communication," *Phys. Commun.*, vol. 63, p. 102286, 2024.

[15] K. Mallikarjunamallu and K. Syed, "Arrhythmia classification for non-experts using infinite impulse response (IIR)-filter-based machine learning and deep learning models of the electrocardiogram," *PeerJ Comput. Sci.*, vol. 10, p. e1774, 2024.

[16] C. Lai and R. Zhao, "An Autocorrelation-Based r-Stability Condition With Application in the Design of IIR Filters," *IEEE Signal Process. Lett.*, 2024.

[17] W. Wang and W. Zhang, "Joint beam training and positioning for intelligent reflecting surfaces assisted millimeter wave communications," *IEEE Trans. Wirel. Commun.*, vol. 20, no. 10, pp. 6282–6297, 2021.

[18] E. Björnson, Ö. Özdogan, and E. G. Larsson, "Intelligent reflecting surface versus decode-and-forward: How large surfaces are needed to beat relaying?," *IEEE Wirel. Commun. Lett.*, vol. 9, no. 2, pp. 244–248, 2019.

[19] R. K. Thenua, A. S. Gandhi, and S. K. Singh, "Sum rate maximization for RIS-assisted NOMA-enabled underlay AmBC-CR networks," *Phys. Commun.*, vol. 64, p. 102358, 2024.

[20] M. Chaudhary and S. K. Bandari, "A low complex joint optimization model for maximizing sum rate and energy efficiency in an IRS-assisted multi-user communication scenario," *Phys. Commun.*, vol. 63, p. 102296, 2024.

[21] C. Huang, Y. Wen, L. Zhang, G. Chen, Z. Gao, and P. Xiao, "Reconfigurable Intelligent Surface Empowered Full Duplex Systems: Opportunities and Challenges," *arXiv Prepr. arXiv2407.15782*, 2024.

[22] A. H. Farah, A. A. Jete, and A. F. Ali, "Propagation Modeling and Performance Analysis on Millimetre Waves for 5G and Beyond Mobile Networks Using OFDM MILLIMETRE WAVES FOR 5G AND BEYOND MOBILE NETWORKS," pp. 0–7, 2025.

[23] Y. Zhang *et al.*, "Cell-free massive MIMO Channels in an Urban Environment -- Measurements and Channel Statistics," pp. 1–13, 2024.

[24] I. E. Lamri, M. Nedil, M. N. E. Temmar, and N. Kandil, "Near-Ground Propagation Channel Modelling and Analysis in Underground Mining Environment at 2.4 GHz," *IEEE Open J. Antennas Propag.*, vol. PP, p. 1, 2025.

[25] P. K. Keer, J. K. S. Al-Safi, S. B. G. T. Babu, and G. Ramesh, "Artificial Intelligence in Computer Network Technology in The Big Data Era," in *2022 5th International Conference on Contemporary Computing and*

Informatics (IC3I), 2022, pp. 2131–2135.
[26] J. Singh, Neeraj, P. Srinivas Reddy, D. S. Hasan, A. T. R. Alsahlanee, and N. Shaik, "IoT-Enabled Automated Smart Irrigation System Incorporating Sensor Parameters," in *Doctoral Symposium on Computational Intelligence*, 2024, pp. 33–43.
[27] A. T. R. Alsahlanee, G. A. Chandhok, T. Saravanan, D. Sugumaran, K. Joshi, and N. Rajesh, "Artificial Intelligence and Machine Learning Approaches based on Power Reduction in Automated Internet of Things Devices," in *2024 International Conference on Advances in Computing, Communication and Applied Informatics (ACCAI)*, 2024, pp. 1–7.
[28] J. Singh, N. A. Shelke, D. S. Hasan, M. Sajid, A. T. R. Alsahlanee, and K. Upreti, "Enhanced Learning in IoT-Based Intelligent Plant Irrigation System for Optimal Growth and Water Management," in *International Conference on Intelligent Systems Design and Applications*, 2023, pp. 231–240.
[29] J. Al-Safi and C. Kaleli, "Item Genre-Based Users Similarity Measure for Recommender Systems," *Appl. Sci.*, vol. 11, no. 13, p. 6108, 2021.
[30] J. K. S. Al-Safi and C. Kaleli, "A Correlation and Slope-Based Neighbor Selection Model for Recommender Systems," in *Next Generation of Internet of Things: Proceedings of ICNGIoT 2021*, 2021, pp. 243–268.
[31] J. Singh, N. P. Singh, B. Vinothkumar, N. A. Shelke, D. Sharma, and A. T. R. Alsahlanee, "Deep Learning Model for Predicting Rice Plant Disease Identification and Classification for Improving the Yield," in *International Conference on Intelligent Systems Design and Applications*, 2023, pp. 138–147.
[32] J. Singh, H. K. Thakur, N. Sharma, A. T. R. Alsahlanee, S. Sahunthala, and N. Shaik, "Deep Learning and Quantum-Enabled Cloud Platform Approach on Optimized Crop Health Predictions," in *Doctoral Symposium on Computational Intelligence*, 2024, pp. 69–80.
[33] J. Singh, M. Dharani, N. A. Shelke[1], and M. Sajid, "Comprehensive Comparative Analysis of Breast Cancer Forecasting Using Machine Learning," *Intell. Syst. Des. Appl. Smart Heal. Vol. 1*, vol. 1, p. 123, 2024.
[34] M. Kulkarni, J. K. S. Al-Safi, S. M. K. S. Reddy, S. B. G. T. Babu, P. Kumar, and P. Pushpa, "Early-Stage Timing Prediction in SoC Physical Design using Machine Learning," in *2023 International Conference on Artificial Intelligence and Knowledge Discovery in Concurrent Engineering (ICECONF)*, 2023, pp. 1–10.
[35] Ö. Özdogan, E. Björnson, and E. G. Larsson, "Intelligent reflecting surfaces: Physics, propagation, and pathloss modeling," *IEEE Wirel. Commun. Lett.*, vol. 9, no. 5, pp. 581–585, 2019.
[36] Q. Wu and R. Zhang, "Intelligent Reflecting Surface Enhanced Wireless Network via Joint Active and Passive Beamforming," *IEEE Trans. Wirel. Commun.*, vol. 18, no. 11, pp. 5394–5409, 2019.
[37] Z.-Q. He and X. Yuan, "Cascaded channel estimation for large intelligent metasurface assisted massive MIMO," *IEEE Wirel. Commun. Lett.*, vol. 9, no. 2, pp. 210–214, 2019.
[38] E. Björnson and L. Sanguinetti, "Demystifying the power scaling law of intelligent reflecting surfaces and metasurfaces," in *2019 IEEE 8th International Workshop on Computational Advances in Multi-Sensor Adaptive Processing (CAMSAP)*, 2019, pp. 549–553.
[39] A. T. Alsahlanee, "Digital Filter Performance Based on Squared Error," in *2021 International Conference on Advanced Computer Applications (ACA)*, 2021, pp. 74–79.
[40] A. T. Alsahlanee, "Convergence Rate For Low-Pass Infinite Impulse Response Digital Filter," *J. Phys. Conf. Ser.*, vol. 1963, no. 1, p. 012103, Jul. 2021.
[41] D. Bratton and J. Kennedy, "Defining a standard for particle swarm optimization," *Proc. 2007 IEEE Swarm Intell. Symp. SIS 2007*, no. Sis, pp. 120–127, 2007.
[42] J. Kennedy and R. Eberhart, "Particle Swarm Optimization," in *Proceedings of ICNN'95-International Conference on Neural Networks*, 1995, vol. 4, pp. 1942–1948.
[43] J. J. Liang and P. N. Suganthan, "Dynamic multi-swarm particle swarm optimizer," *Proc. - 2005 IEEE Swarm Intell. Symp. SIS 2005*, vol. 2005, pp. 127–132, 2005.
[44] D. Sanchez, "DS-PSO : Particle Swarm Optimization with Dynamic and Static Topologies," *Bowdoin Coll. Bowdoin Digit. Commons, Honor. Proj.*, 2017.